



A EUROPEAN JOURNAL OF CHEMICAL BIOLOGY

CHEM **BIO** CHEM

SYNTHETIC BIOLOGY & BIO-NANOTECHNOLOGY

Accepted Article

Title: Biochemical Characterization of Intact Oncogenic BRAFV600E Together With Molecular Dynamics Simulations Provide Insight into the Activation and Inhibition Mechanisms of RAF Kinases

Authors: Nicholas Cope, Borna Novak, Christine Candelora, Kenneth Wong, Maria Cavallo, Amber Gunderwala, Zhiwei Liu, Yana Li, and Zhihong Wang

This manuscript has been accepted after peer review and appears as an Accepted Article online prior to editing, proofing, and formal publication of the final Version of Record (VoR). This work is currently citable by using the Digital Object Identifier (DOI) given below. The VoR will be published online in Early View as soon as possible and may be different to this Accepted Article as a result of editing. Readers should obtain the VoR from the journal website shown below when it is published to ensure accuracy of information. The authors are responsible for the content of this Accepted Article.

To be cited as: *ChemBioChem* 10.1002/cbic.201900266

Link to VoR: <http://dx.doi.org/10.1002/cbic.201900266>

WILEY-VCH

www.chembiochem.org

A Journal of



Biochemical Characterization of Full-Length Oncogenic BRAF^{V600E} Together with Molecular Dynamics Simulations Provide Insight into the Activation and Inhibition Mechanisms of RAF Kinases

Nicholas Cope¹, Borna Novak¹, Christine Candelora¹, Kenneth Wong¹, Maria Cavallo¹, Amber Gunderwala¹, Zhiwei Liu¹, Yana Li², and Zhihong Wang^{*,1}

¹ Department of Chemistry & Biochemistry, University of the Sciences, Philadelphia, PA 19104, United States

² Eukaryotic Tissue Culture Facility, Johns Hopkins University School of Medicine, Baltimore, MD 21205, United States

Abstract: The most prevalent BRAF mutation, V600E, occurs frequently in melanoma and other cancers. Although extensive progress has been made toward understanding the biology of RAF kinases, little *in vitro* characterization of full-length BRAF^{V600E} is available. Here, we show successful purification of active, full-length BRAF^{V600E} from mammalian cells for *in vitro* experiments. Our biochemical characterization of intact BRAF^{V600E} together with molecular dynamics (MD) simulations of BRAF kinase domain and cell-based assays demonstrate that BRAF^{V600E} has several unique features that attribute to its tumorigenesis. First, steady-state kinetic analyses reveal that purified BRAF^{V600E} is more active than fully-activated wild-type BRAF, consistent with the notion that elevated signaling output is necessary for transformation. Second, BRAF^{V600E} has a higher potential to form oligomers, despite the fact that the V600E substitution confers constitutive kinase activation independent of an intact side-to-side dimer interface. Third, BRAF^{V600E} bypasses inhibitory P-loop phosphorylation to enforce necessary elevated signaling output for tumorigenesis. Together, we provide new insight into the biochemical properties of BRAF^{V600E}, complementing the understanding of BRAF regulation under normal and disease conditions.

Introduction:

The RAS/RAF/MEK/ERK signal transduction pathway, also called the mitogen-activated protein kinase (MAPK) cascade, controls vital cellular processes such as cell proliferation and differentiation under physiological conditions and is often dysregulated in human cancers.^[1] In normal cells, the MAPK cascade is activated by mitogens such as growth factors, cytokines, and hormones, which bind to and activate specific receptors on the cell surface. The strength and duration of signals processed through the MAPK pathway are mainly regulated by the upstream elements, in particular by the RAF serine-threonine kinase family. The RAF family comprises three homologs in human: ARAF, BRAF, and CRAF. In their inactive state, RAF kinases exist in the cytosol in a closed monomeric conformation, with the N-terminal regulatory domains interacting with and autoinhibiting the C-terminal kinase domain.^[2] According to the currently accepted model, the first step in the RAF activation process is recruitment of RAF to the plasma membrane by receptor-activated RAS, in which binding of GTP-loaded RAS to the N-terminal RAS-binding domain of RAF brings RAF kinases into close proximity.^[3] The RAS/RAF interaction relieves autoinhibitory interactions to induce RAF homo- and/or heterodimerization between two kinase domains that enables allosteric activation of its cognate partner.^[4] To achieve maximal kinase activity, its activation loop requires phosphorylation.^[5] Once activated, RAF kinase phosphorylates and activates the dual-specificity kinase MEK1/2, which in turn phosphorylates and activates ERK1/2 to relay the signals throughout the cell.

BRAF seems to be the major MAPK effector, as it has higher basal activity than ARAF and CRAF.^[6] Adding to its importance, BRAF mutations occur frequently in a variety of cancers while ARAF and CRAF mutations are very rare.^[7] BRAF mutations are prevalent in melanoma (~66%), thyroid cancer (~70%), ovarian cancer (~30%), and colorectal cancer (~20%),^[7] which makes BRAF a target for therapeutic intervention in human cancer. To date, BRAF is the most successful drug target among the core components of the MAPK cascade. The most common oncogenic BRAF mutation is the V600E mutation, which accounts for more than 90% of all BRAF mutations. Oncogenic BRAF^{V600E} is constitutively active and stimulates the MAPK pathway independently of mitogenic activation and RAS.^[8] Targeting BRAF with ATP-competitive inhibitors vemurafenib and dabrafenib yields unprecedented response rates in melanoma patients harboring the V600E BRAF mutation.^[9] However, the same BRAF inhibitors unexpectedly provoke the so-called paradoxical activation of MAPK signaling and induce secondary malignancies in melanoma patients carrying activating RAS mutations.^[10] These concerns surrounding current BRAF inhibitor therapy underscore the need for further investigation to elucidate the mechanisms that modulate the MAPK signaling.^[11]

The catalytic domain of all eukaryotic protein kinases share a small N-terminal lobe (N-lobe) and a large C-terminal lobe (C-lobe) linked by a hinge region.^[12] The N-lobe contains an α helix called the " α C-helix". The C-lobe contains a flexible activation loop, which starts with a conserved Asp-Phe-Gly ("DFG") motif. The α C-helix and the activation loop, including the DFG motif, undergo significant conformational changes to transit a kinase between active and inactive states during catalysis. For example, the activation loop, once phosphorylated, typically adopts a fully extended configuration to stabilize the active conformation of kinase.^[13] Investigation and comparison of various crystal structures throughout the kinome have identified that the α C-helix and the DFG motif can adopt either an "IN" or "OUT" position, corresponding to an active or inactive conformation of the kinase domain respectively. In most kinases, the "IN" position of α C-helix and DFG locks the kinase in the active conformation. In addition, occupancy of RAF inhibitors within the BRAF kinase domain has been correlated with the orientation of the α C-helix.^[14] Structurally diverse RAF inhibitors preferentially stabilize different conformations and thus are classified into three categories, α C-helix-IN/DFG-IN, α C-helix-IN/DFG-OUT, and α C-helix-OUT/DFG-IN.^[15]

Extensive structural and biochemical studies on the kinase domain of BRAF revealed phosphorylation of key residues and dimerization of the kinase domain as two essential mechanisms of BRAF kinase activation.^[14a] The structure of monomeric BRAF kinase domain revealed that the activation loop forms a short helix, termed helix AS-H1, that packs against α C-helix to maintain the inactive conformation of BRAF.^[16] Furthermore, the hydrophobic interactions between the activation loop and the phosphate-binding loop (P-

loop) were speculated to stabilize the inactive conformation.^[8] Phosphorylation of Thr599 and Ser602 within the activation loop is believed to destabilize these interactions, causing full activation of BRAF. The V600E mutation lies in the activation loop of BRAF and contributes to BRAF activation independent of RAS binding. Substitution of hydrophobic Val600 with negatively charged glutamate is believed to mimic phosphorylation of the activation loop. A salt bridge between E600 and K507 of the α C-helix is observed to stabilize the active kinase conformation,^[9b, 16] which may explain in part the high kinase activity of this BRAF mutant. The mechanism by which dimerization leads to BRAF activation is only partially understood, but it is likely that one kinase allosterically activates the other kinase within the dimer.^[4a] Dimerization of RAF kinases involves a highly conserved 'side-to-side' dimer interface within the kinase domain.^[4a] Disruption of this dimer interface via the R509H mutation has been reported to result in BRAF inactivation.^[17] Intriguingly, artificial dimerization of BRAF^{R509H} failed to rescue the kinase activity of BRAF,^[4a] highlighting the significance of this 'side-to-side' dimer interface. Phosphorylation of the glycine-rich P-loop negatively regulates the catalytic activity of wild-type BRAF and CRAF *in vitro*.^[18] The P-loop is one of the two hotspots of BRAF mutations,^[7] further supporting that P-loop plays an important role in regulating the RAF kinase activity. From structural studies of other protein kinases, the P-loop region anchors the β - and γ - phosphates of ATP and may orientate ATP for phosphate transfer.^[19] However, the functional significance of P-loop phosphorylation in regulating oncogenic BRAF mutants has not been investigated.

Despite the extensive interest in developing inhibitors targeting BRAF^{V600E}, the potential role of V600E mutation in oncogenic activation and drug sensitivity is not fully understood. Most *in vitro* BRAF studies reported to date used the catalytic domain, which we have shown to be less active and a poor physiological replicate compared to full-length BRAF.^[5b] Biochemical characterization of purified full-length oncogenic BRAF reported here complements current knowledge obtained from truncated kinase domain and cell-based studies. Moreover, molecular dynamics simulations of BRAF^{V600E} kinase domain provide compelling evidence for enhanced dimerization potential of BRAF^{V600E}. A better understanding of the mechanisms of oncogenic activation may guide the development of novel BRAF inhibitors.

Results:

Purification of Full-Length BRAF^{V600E} from HEK293F Mammalian Cells.

To obtain full-length (FL) BRAF^{V600E}, we transiently expressed Flag-tagged FL-BRAF^{V600E} in HEK293F cells, a mammalian expression system proved to be optimal for expression of functional FL-kinases in the past.^[20] The protein was purified through affinity and size exclusion chromatography. As shown in Figure 1A, the elution profile after size exclusion chromatography revealed three peaks, corresponding to aggregate, higher-order oligomer, and dimer, respectively. We collected them separately and identified that they display similar kinetic parameters toward phosphorylating kinase-dead MEK1 *in vitro* regardless of oligomer status (Supplementary Figure S1). Since the majority (> 70%) of purified protein eluted as the second and third peaks, we combined the two protein fractions and used them for all the kinase assays conducted in this study. The purity of concentrated BRAF protein is above 80%, suitable for *in vitro* kinetics studies (Figure 1B). We realized that BRAF^{V600E} co-purified with a trace amount of HSP70 (Figure 1B). Our previous results have demonstrated that the presence of HSP70 has no impact on enzyme kinetics.^[5b] In addition, the smaller bands corresponding to ~50 kDa were identified by mass spectrometry to be fragments of BRAF and no kinase activity was detected for those fragments. For comparison, we purified truncated catalytic domain of BRAF^{V600E} from insect cells, which is widely used by other laboratories to evaluate the IC₅₀ values of RAF inhibitors. The specific activity of FL-BRAF^{V600E} is ~ 10-fold higher than that of catalytic domain purified from insect cells (Figure 1C). It is possible that different post-translational modifications from the two expression systems contribute to the observed discrepancy. Regardless, the full-length BRAF we obtained is more active and thus is advantageous for *in vitro* biochemical characterization of BRAF.

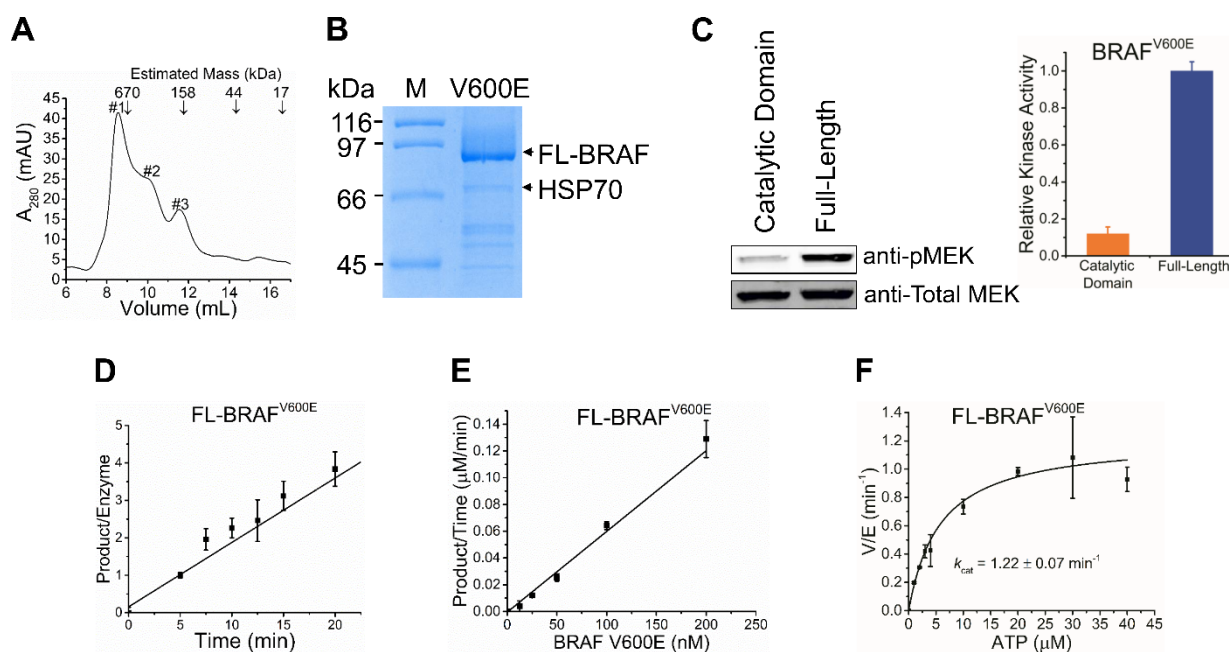


Figure 1 Purification and Enzymatic Analyses of FL-BRAF^{V600E}. **A**) Size-exclusion chromatography of purified FL-BRAF^{V600E}. Elution volumes of protein standards (670, 158, 44, and 17 kDa) are indicated by arrows. **B**) Purified FL-BRAF^{V600E} was analyzed by coomassie blue-stained SDS-PAGE. FL-BRAF^{V600E} and HSP70 bands are highlighted with arrows. The molecular weight marker (M) and FL-BRAF^{V600E} are shown above the gel. **C**) Activity comparison of 5 nM FL- or catalytic domain BRAF^{V600E} with 100 μ M ATP and 100 nM MEK. Reaction solutions were exposed to Western blot analysis with anti-pMEK antibody (left). Steady-state radioactive kinetic analyses of FL-BRAF^{V600E}. Enzyme activity is linear with **D**) reaction time (0, 5, 7.5, 10, 12.5, 15, and 20 min) and **E**) enzyme concentration

(0, 12.5, 25, 50, 100, 200 nM). F) FL-BRAF^{V600E} values of K_m for ATP and k_{cat} were acquired by changing the ATP concentrations (0, 1, 2, 3, 4, 10, 20, 30, and 40 μ M) with constant BRAF (50 nM) and MEK (350 nM) enzyme concentrations. The reaction was performed at 30°C for 5 minutes. The quantification of pMEK signal (Relative Kinase Activity) for all experiments were performed with ImageJ software. The bar graph/points symbolize the averages of at least 3 independent replicates \pm S.D.

Steady-State Kinetics of FL-BRAF^{V600E}.

Steady-state kinetics of FL-BRAF^{V600E} was performed using previously developed radioactive kinase assays, in which the consumption of ATP was monitored as the readout of BRAF activity and kinase-dead FL-MEK1 purified from *E. coli* was used as the phosphorylated substrate.^[5b] As shown in Figure 1D&E, the reaction rate is linear *versus* reaction time and enzyme concentration, supporting that the reactions catalyzed by BRAF under the conditions of our assay meet the prerequisite for steady-state kinetics. Subsequently, we chose BRAF enzyme concentration of 50 nM, a saturating MEK1 substrate concentration of 350 nM (K_m for MEK1 is 55 nM), and reaction time of 5 min for the following steady-state kinetics. The apparent activities were plotted against various substrate concentrations and fitted according to the Michaelis–Menten equation. The determined parameters k_{cat} and K_m for substrates are shown in Figure 1F (ATP K_m), Supplementary Figure S2 & Table 1. The k_{cat} value of BRAF^{V600E} is 3-fold higher than that of wild-type BRAF (Table 1); however, previous cell-based assays demonstrate that oncogenic BRAF^{V600E} is 700-fold more active than basal wild-type BRAF.^[8] We believe that this discrepancy is due to the fact that our *in vitro* assays quantified the activity of purified FL-wild-type, which is dimeric and constitutively active in solution, unlike wild-type BRAF expressed in cells which is under control of multiple negative regulation mechanisms. In addition, we suspect that BRAF^{V600E} has other mechanisms to maintain abnormally high kinase activity in cells, such as evading negative feedback regulation. The V600E mutant and wild type have a similar K_m value for MEK substrate, suggesting that MEK binding is less likely to be affected by the activation loop mutation.

Table 1: Full-length BRAF Kinetic Parameters

FL-BRAF	MEK K_m (nM)	ATP K_m (μ M)	k_{cat} (min^{-1})	$k_{cat}/K_m, ATP$ ($\text{min}^{-1} \mu\text{M}^{-1}$)
WT ^[5b]	53.43 \pm 3.11	6.64 \pm 1.50	0.44 \pm 0.03	0.07
V600E	54.56 \pm 9.45	3.54 \pm 0.27	1.22 \pm 0.07	0.34
V600E/R509H	52.03 \pm 10.22	12.75 \pm 4.27	ND	ND

Table 2: IC₅₀ Values of Various ATP Competitive Inhibitors

Inhibitor	FL- V600E (nM)	CD-V600E (nM)	FL- Wild-Type (nM) ^[5b]	FL- V600E/R509H (nM)	α C-Helix /DFG
Vemurafenib	3.36 \pm 1.56	59.64 \pm 9.43	21.2	ND	OUT/IN
Dabrafenib	0.77 \pm 0.01	1.57 \pm 1.09	50	0.55 \pm 0.04	OUT/IN
PB-PLX7904	14.13 \pm 1.34	2.05 \pm 0.63	15.45 \pm 2.86	ND	OUT/IN
TAK-632	0.94 \pm 0.08	8.31 \pm 3.92	0.70 \pm 0.02	ND	IN/OUT
AZ-628	0.86 \pm 0.18	3.02 \pm 1.45	ND	0.35 \pm 0.04	IN/OUT
SB-590885	0.63 \pm 0.05	0.38 \pm 0.13	0.11 \pm 0.06	4.34 \pm 0.25	IN/IN

The V600E mutation decreases the K_m for ATP ~2-fold, as compared with wild-type BRAF. Although such a modest change is unlikely to impact kinase activity under physiological ATP concentrations (~ 1 mM), this subtle difference in the ATP-binding pocket might contribute to distinct drug selectivity. BRAF inhibitors have been classified into three categories, α C-helix-IN/DFG-IN, α C-helix-IN/DFG-OUT, and α C-helix-OUT/DFG-IN,^[15] based on the position of α C-helix and DFG motif within the kinase domain bound with each inhibitor. We measured the IC₅₀ values of three types of BRAF inhibitors against the V600E mutant, using an ELISA assay in which phosphorylated MEK1 was quantified *via* phospho-specific antibody. As shown in Table 2 & Figure S3, different from wild-type BRAF,^[5b] the V600E mutant is potently inhibited by all three categories of RAF inhibitors, regardless the position of the α C-helix and DFG motif. The biochemical selectivity towards V600E revealed here has been demonstrated to translate to cellular selectivity in V600E mutant tumors.^[21] Previously, we observed that dabrafenib and vemurafenib paradoxically activate purified FL-wild-type BRAF.^[5b] Consistent with cellular and *in vivo* data, purified FL-BRAF^{V600E} didn't display paradoxical activation toward dabrafenib and vemurafenib, suggesting that the potential structural perturbation introduced by the V600E mutation plays a role in evading paradoxical activation.

Interestingly, in comparison with the catalytic domain of BRAF, FL-BRAF displays a different inhibition profile. As shown in Table 2, the IC₅₀ value of vemurafenib against FL-BRAF^{V600E} is 17-fold lower than that of catalytic domain. Although the binding site of ATP-competitive inhibitors is deeply buried inside the catalytic domain, our data strongly demonstrate that the regulatory domains of BRAF exert long-distance allosteric effects on the active site of kinase domain, therefore it is necessary to include the regulatory domains in biochemical characterization of RAF kinases.

The V600E Mutation Renders Higher Oligomerization Potential.

The observed higher-order oligomer by size exclusion chromatography analysis led us to suspect that the hydrophobicity of the N-terminal regulatory domains might be the cause. However, we have identified that FL-wild-type BRAF dominantly forms dimers in

solution.^[5b] Similarly, previous analytical ultracentrifugation analysis of BRAF catalytic domain demonstrated that V600E has enhanced dimerization potential, relative to wild-type BRAF.^[16, 22] We suspect that this feature of BRAF^{V600E} protects against negative regulators such as CRAF, which has been shown to inhibit the oncoprotein through formation of the BRAF/CRAF complex.^[23] Together, we believe that the V600E mutation promotes oligomerization of BRAF. Since the effect of phosphorylation is similar to glutamate substitution, activation loop phosphorylation might be also critical for triggering dimerization of wild-type BRAF.

MD Simulations of the V600E and Wild-Type Kinase Domain.

The crystal structures of BRAF^{V600E} kinase domain all display as a dimer, similar to many of the solved wild-type structures, thus it is not clear how the V600E mutation alters the conformation of BRAF to prompt constitutive activation and higher dimerization potential. In addition, all the available crystal structures are bound with a variety of BRAF inhibitors, which are known to impact the structural conformation. In light of this, we carried out MD simulations to access the conformational dynamics of monomeric V600E kinase domain and monomeric wild-type BRAF kinase domain in aqueous solution and in the absence of BRAF inhibitor. The starting structures of these two simulations are the crystal structures for dimeric BRAF^{V600E} kinase domain in complex with vemurafenib (PDB entry 3OG7^[9b]) and monomeric wild-type BRAF kinase domain in complex with PLX-4720 (PDB entry 4WO5^[16]). After extracting one BRAF^{V600E} protomer from the BRAF^{V600E} dimer, we removed the bound inhibitor and carried out the MD simulations in solution. In parallel, wild-type apo-BRAF was simulated in the same way. The overlay of BRAF^{V600E} monomer and wild-type BRAF monomer shows that the α C-helix of V600E is ~ 5 Å closer to the C-lobe of the kinase domain (Figure 2A&B; Figure 3A), suggesting that monomeric V600E mutant prefers the active α C-helix IN conformation while the monomeric wild-type adopts an inactive α C-helix OUT conformation. RAF kinases dimerize via the C-terminal end of the α C-helix, thereby side-to-side dimerization and position of the α C-helix are reciprocally coupled to each other, i.e. dimer possesses the α C-helix IN conformation.^[24] Our MD simulation analyses clearly indicate that the V600E mutation favors the α C-helix IN orientation, which should not only stabilize the active conformation, but also results in a higher oligomerization potential. Furthermore, throughout the MD trajectory (100 to 150 ns), the activation loop of V600E is fully extended while the activation loop of wild-type maintains a short helix, referred as AS-H1 (Figure 2C), consistent with the crystallographic data reported by Thevakumaran *et al.*,^[16] implicating that the V600E alteration induces unfolding of the short helix to relieve auto-inhibition interactions.

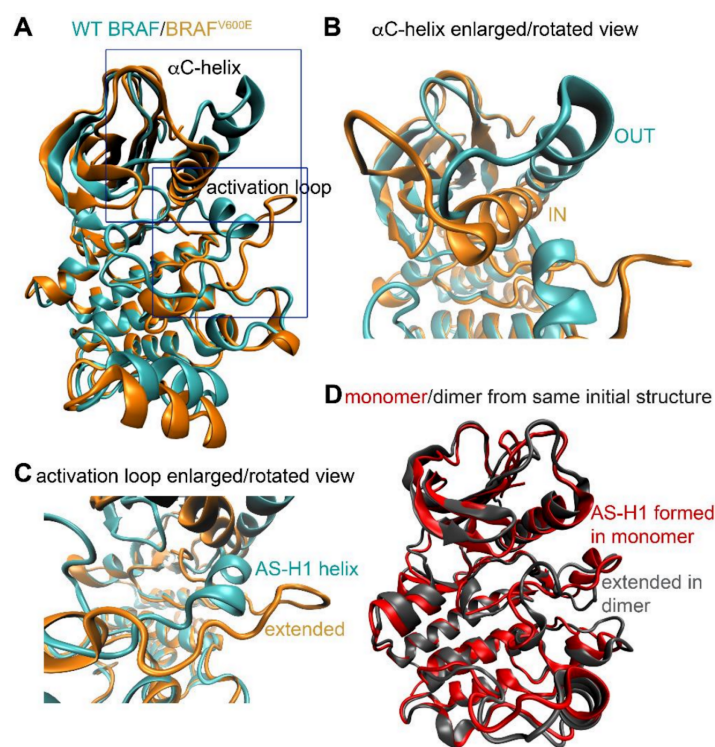


Figure 2 Structural Comparison of Monomeric BRAFWT and BRAF^{V600E} through MD Simulations. **A)** Overlay of the representative snapshots of wild-type BRAF monomer (cyan) and BRAF^{V600E} monomer (orange) from MD simulations that start from the crystal structure 4WO5 and 3OG7, respectively. **B)** Enlarged view of the α C-helix region. **C)** Enlarged view of the activation loop region. **D)** Overlay of the representative snapshots of wild-type BRAF monomer (red) and dimer (gray, only one protomer shown) from MD simulations that start from the dimer crystal structure 4E26.

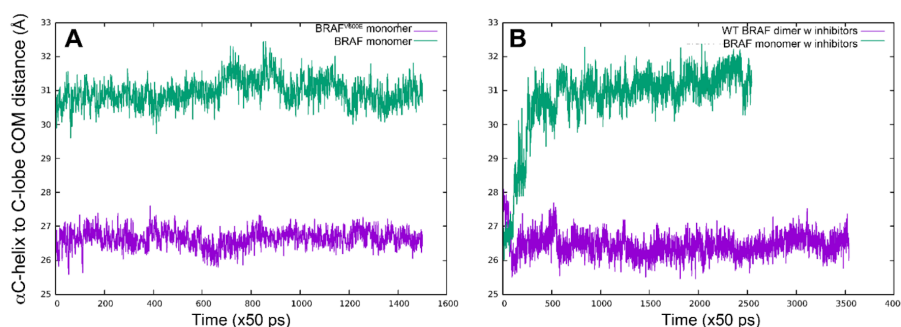


Figure 3 The distance between the α C-helix and the C-lobe. Molecular dynamics trajectory indicating center of mass (COM) distance from the α C-helix to the C-lobe as a function of time. **A**) Simulations of BRAF^{V600E} monomer (purple) started from the crystal structure of dimeric BRAF^{V600E} (PDB entry 3OG7) and simulations of BRAF^{WT} monomer (green) started from the crystal structure of monomeric wild-type BRAF (PDB entry 4WO5). **B**) Simulations of inhibitor-bound BRAF^{WT} monomer (green) and inhibitor-bound BRAF^{WT} dimer (purple), both of which started from the crystal structure of dimeric wild-type BRAF (PDB entry 4E26).

To verify that MD simulations are feasible to capture dynamic structural changes upon removing one protomer from a dimer, we applied the same approach to wild-type BRAF dimer. We carried out the following two simulations: another wild-type monomer system with initial structure extracted from the crystal structure of wild-type dimer (PDB entry 4E26^[25]) by removing one protomer and the bound inhibitor, and the wild-type dimer system without inhibitors starting from the same crystal structure (4E26). The representative snapshots of the two systems were overlaid to highlight the distinct features (Figure 2D). Indeed, the monomer simulation that started from an active “dimer” crystal structure with extended activation loop showed formation of the short AS-H1 helix within 100 ns (Figure 2D). The activation loop usually adopts an extended state to stabilize the active conformation.^[13] This is a clear tendency of switching from the initial active conformation of “dimer” to an inactive conformation of monomer. In contrast, simulations of the wild-type dimer system demonstrated that the dimer remained as the active conformation in the absence of inhibitors (Figure 2D), supporting that the formation of the short AS-H1 helix is caused by dimer dissociation, not by removal of bound inhibitor. These simulations further validated the results from the BRAF^{V600E} and wild-type BRAF monomer simulations. Consistent with the notion that conformational changes of the activation loop are typically coupled to the movements of α C-helix, we observed that the α C-helix within the monomer system is less stable and is moving apart from the C-lobe to adopt the “OUT” position (Figure 3B). Moreover, the results confirmed that the ‘side-to-side’ dimer facilitates wild-type BRAF adopting the active conformation, providing structural evidence for allosteric transactivation.

Role of the ‘Side-to-Side’ Dimer Interface on Oncogenic BRAF^{V600E}

The activity of purified BRAF^{V600E} kinase domain was abolished by the R509H mutation.^[16, 26] However, the kinase activity of FL-BRAF^{V600E} expressed in cells was not affected by the R509H mutation that is known to severely disrupt the ‘side-to-side’ dimer interface.^[27] It remains controversial whether the V600E mutation causes abnormally high activity primarily by promoting constitutive dimerization and activation of BRAF or rendering dimer-independent BRAF activation. To investigate the functional role of the ‘side-to-side’ dimer interface, we purified FL-BRAF^{V600E/R509H} from HEK293F cells (Figure 4A). Distinct from previous studies on isolated kinase domain, the specific activity of FL-BRAF^{V600E/R509H} was only decreased by 40% after introducing the R509H mutation (Figure 4B), indicating that BRAF^{V600E} does not require an intact ‘side-to-side’ dimer interface to be catalytically active. Such a marginal difference between BRAF^{V600E} and BRAF^{V600E/R509H} *in vitro* explains why no significant difference in MAPK signaling was detected by cell-based assays (Figure 4C).^[26]

Both cell-based co-immunoprecipitation of FL-BRAF^{V600E/R509H} and *in vitro* biophysical characterization of purified BRAF^{V600E/R509H} kinase domain support that the R509H mutation dissociates BRAF^{V600E} dimer.^[26] To verify that purified FL-BRAF^{V600E/R509H} indeed has a disrupted dimer interface, we incubated FL-BRAF^{V600E} and FL-BRAF^{V600E/R509H} with P³²-labelled ATP and MEK substrate for 30 min at 30°C to let phosphorylation occur. The incorporation of P³² into BRAF and MEK was recorded simultaneously *via* autoradiograph. As shown in Figure 4D, BRAF^{V600E} phosphorylated itself and MEK, however, BRAF^{V600E/R509H} only phosphorylated MEK. Similarly, Western blotting analysis demonstrated that autophosphorylation of the activation loop (pThr599), using a phospho-specific antibody (Figure S4), only occurred to BRAF^{V600E}, not to BRAF^{V600E/R509H} (Figure 4E). Evidently, the R509H mutation does disrupt the ‘side-to-side’ dimer interface of FL-BRAF^{V600E} to abolish FL-BRAF^{V600E/R509H} autophosphorylation. In addition, we provide strong evidence to support that BRAF autophosphorylation occurs in *trans*, not *cis*, thus requires an intact dimer interface. Together, our biochemical data clearly demonstrate that the kinase activity of oncogenic BRAF^{V600E} is not contingent on the ‘side-to-side’ dimer that is necessary for wild-type RAF activation. Apparently, the V600E substitution is sufficient to stabilize the active conformation without formation of the ‘side-to-side’ dimer. Our MD results, of which the BRAF^{V600E} monomer maintains the α C-helix IN and extended activation loop conformation, also support the conclusion.^[17]

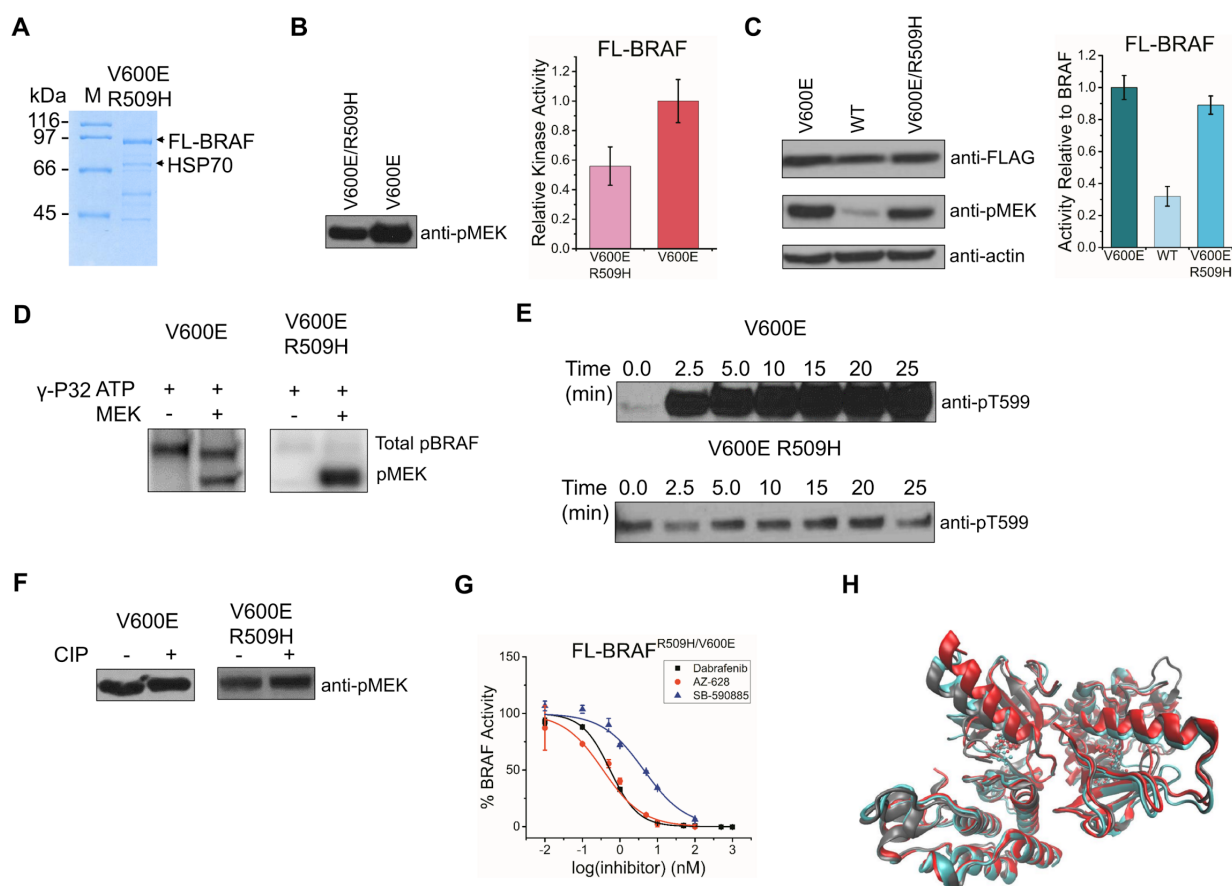


Figure 4 BRAF^{V600E} Requires an Intact Dimer Interface for *trans*-Autophosphorylation but not for Catalytic Activity. **A)** Purified FL-BRAF^{V600E/R509H} was analyzed by Coomassie blue-stained SDS-PAGE. FL-BRAF^{V600E/R509H} and the molecular weight marker (M) are indicated above the gel. FL-BRAF^{V600E/R509H} and HSP70 are indicated by arrows. **B)** Quantification of the activities of 5 nM FL-BRAF^{V600E/R509H} and FL-BRAF^{V600E} with 100 μ M and 100 nM MEK. Reactions were subjected to Western blot analysis with anti-pMEK antibody. **C)** BRAF^{V600E}, BRAF^{WT}, and BRAF^{V600E/R509H} were transiently transfected into HEK293F cells. The cells were lysed in 4% SDS and subjected to Western blot testing for anti-FLAG (BRAF), anti-pMEK, and anti-actin antibodies. Relative kinase activity denotes the relative signal intensity compared to V600E. Activity relative to BRAF is the pMEK intensity divided by the BRAF (FLAG) intensity. Bar graphs represent the average \pm S.D. Evaluating the phosphorylation of FL-BRAF^{V600E} (left) and FL-BRAF^{V600E/R509H} (right). **D)** Autoradiograph phosphorimage screening the transfer of radioactive phosphate (³²P) to BRAF or MEK concurrently of FL-BRAF^{V600E} or FL-BRAF^{V600E/R509H}. 100 nM BRAF, 100 μ M cold ATP and 1 μ Ci radioactive ATP were incubated without or with 350 nM MEK for 30 min at 30 °C. The bands for autophosphorylated BRAF (top) or phosphorylated MEK (bottom) are indicated. The quantification of these blots were performed with Image J software and bar graphs are shown to the right with three independent experiments averaged \pm S.D. The activation loop was monitored with pT599 antibody for **E)** FL-BRAF^{V600E} and FL-BRAF^{V600E/R509H} over a time course of 0-25 minutes. **F)** Assessment of dephosphorylated or native BRAF. Dephosphorylated BRAF was achieved after incubation with CIP protein phosphatase. Native protein was purified from HEK293F cells. **G)** ATP-competitive inhibitor IC₅₀ curves for FL-BRAF^{R509H/V600E}. **H)** Alignment of BRAF^{V600E} catalytic domain crystal structures bound to ATP-competitive inhibitors: Dabrafenib PDB 4XV2 (red), GDC-0879 PDB 4MNF (gray), and LY-3009120 PDB 5C9C (cyan).

Consistent with the notion that phosphorylation of the activation loop is required for wild-type BRAF activation, dephosphorylated wild-type BRAF is not able to phosphorylate MEK substrate.^[5b] Within a BRAF dimer, BRAF *trans*-phosphorylates the activation loop to further enhance BRAF activity. Our finding highlights another physiological significance of the ‘side-to-side’ dimer interface, other than allosteric transactivation. The kinase activities of BRAF^{V600E} and BRAF^{V600E/R509H} were not affected by dephosphorylation (Figure 4F), further supporting that negatively charged glutamate side chain is sufficient to stabilize the active conformation regardless of activation loop phosphorylation.^[5c] In addition, the discrepancy between catalytic domain and FL of BRAF further supports our view that studying FL-BRAF is advantageous over truncated kinase domain.

The V600E Alteration Confers Drug Selectivity.

Dimerization of BRAF has been correlated with reduced drug sensitivity,^[26] however, other studies suggest that enhanced association with MEK, not dimerization of BRAF, attributes to drug resistance.^[29] To investigate whether dimerization of FL-BRAF^{V600E} impacts drug sensitivity, we took advantage of that oligomeric BRAF^{V600E} and monomeric BRAF^{V600E/R509H} have comparable activities in their purified form and measured the IC₅₀ values of three structurally diverse BRAF inhibitors against them *in vitro*. Similar potency in inhibiting monomeric BRAF^{V600E/R509H} and dimeric BRAF^{V600E} is observed for AZ-628 and SB-590885 (Figure 4G&Table 2), which is consistent with the solved structures in which α C-helix-IN inhibitors are compatible for occupying the two drug binding sites within BRAF dimer.^[17, 30] Dabrafenib is believed to stabilize the ‘OUT’ position of the α C-helix, thus sterically prevents from occupying both of the drug binding sites in the context of wild-type BRAF. This negative allostery explains why α C-helix-OUT/DFG-IN inhibitors are less potent against wild-type BRAF.^[14] Intriguingly, disruption of the dimer interface does not further increase the inhibition potency of dabrafenib against BRAF^{V600E} (Figure 4G&Table 2). To understand this discrepancy, we overlaid the reported structures of dimeric BRAF^{V600E} bound to dabrafenib^[31] and two α C-helix-IN inhibitors (GDC-0879^[17] and LY3009120^[30]) (Figure 4H). Surprisingly, the two dabrafenib-bound protomers adopt different configurations, one is α C-helix-OUT and the other is α C-helix-IN. These observations suggest that dabrafenib is compatible with both conformations and does not display negative allostery in the context of dimeric BRAF^{V600E}.

BRAF^{V600E} Bypasses Inhibitory Phosphorylation in Cells.

Two residues Ser357/Ser359 in the P-loop region of CRAF were reported to negatively regulate CRAF upon phosphorylation.^[18] Whether the two corresponding residues Ser465/Ser467 (equivalent to Ser357/Ser359 on CRAF) in the P-loop region of BRAF have the same effect on oncogenic BRAF is unclear. We speculate that this negative feedback loop is lost in tumor cells carrying oncogenic mutations that render constitutive activation of BRAF. In light of this, we introduced Ala and Asp to replace Ser465/Ser467 to mimic unphosphorylated and phosphorylated P-loop, respectively. After transfection of the two constructs, referred to SS/AA and SS/DD, into HEK293 cells, the cellular activity of BRAF was examined by probing for phosphorylated MEK. The introduction of SS/DD mutation significantly inhibits the kinase activity of both wild type and V600E (Figure 5A&B), supporting that P-loop phosphorylation plays an inhibitory role. In the context of wild-type BRAF, SS/AA mutation prevents inhibitory P-loop phosphorylation, thus increases BRAF kinase activity by ~50%, as shown in Figure 5A&B, further verifying that P-loop phosphorylation negatively regulates BRAF kinase activity.

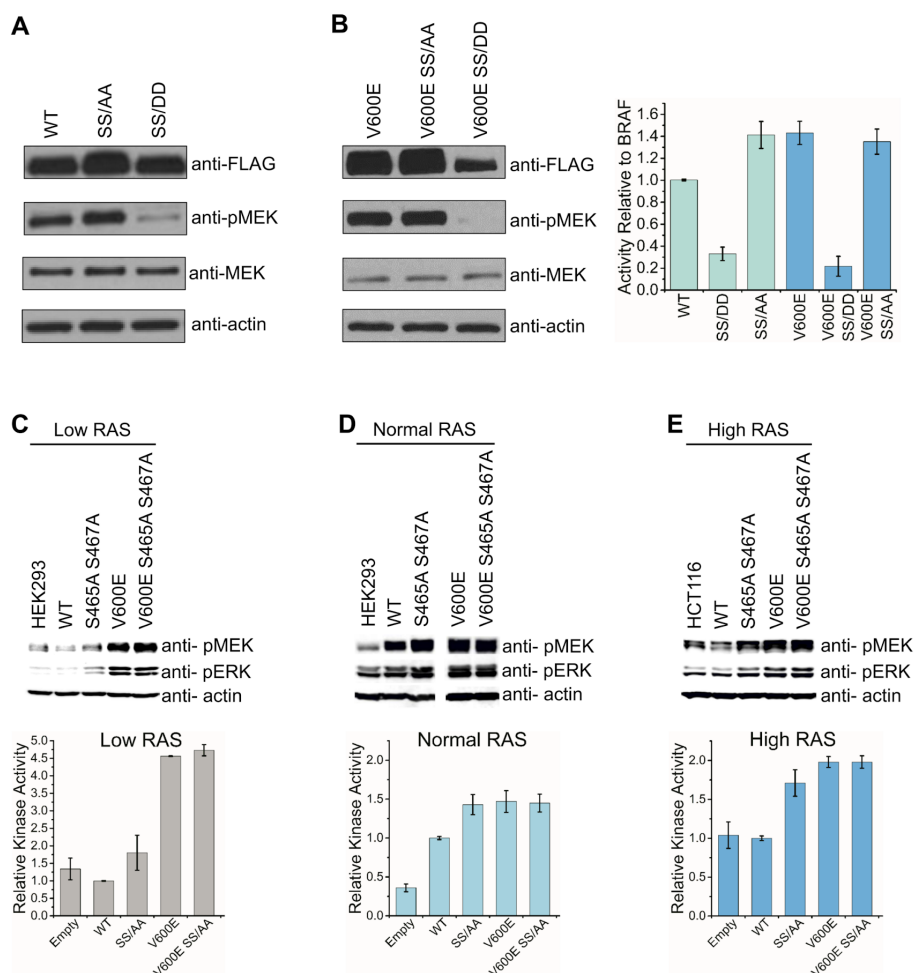


Figure 5. BRAF^{V600E} Escapes Inhibitory P-loop Phosphorylation. Cell-based analysis of BRAF P-loop mutations in HEK293 cells. The phospho-mimetic double mutation SS/DD (S465D/S467D) and an aliphatic SS/AA (S465A/S467A) double mutation were inserted into **A**) Wild-type BRAF and **B**) BRAF^{V600E}. The cells were lysed with 4% SDS then subjected to Western blot analysis and immunoblotted with pMEK and FLAG (BRAF) antibodies. The relative intensities are relative to wild-type BRAF for all lanes. The activity relative to BRAF represents the pMEK signal divided by the amount of BRAF loaded in that lane. The bars represent the average \pm S.D. RAS activity has no effect on monomeric or dimeric BRAF^{V600E} signaling. We assessed BRAF WT, SS/AA, V600E, and V600E SS/AA at **C**) low, **D**) medium, or **E**) high RAS activities. To obtain low RAS signaling we serum starved HEK293 cells in DMEM without FBS for four hours. For high RAS activity cells, we introduced our constructs into cancer cells (HCT116) that are expressing active KRAS^{G13D}. The quantitation of the Western blot images for low, normal, and high RAS activities are shown. The relative kinase activity were calculated by dividing the intensities of pMEK by actin for each respective lane. The bar graph represents the average of at least three replicates \pm S.D. The Western blot intensity values were quantified with ImageJ. Relative kinase activity represents the average Western blot anti-pMEK antibody signal of three independent experiments \pm S.D.

Intriguingly, the SS/AA mutation has a distinct effect on the V600E mutant. As shown in Figure 5B, BRAF^{V600E} and BRAF^{V600E} SS/AA displayed similar kinase activity in transiently transfected HEK293 cells. To rule out the possibility that the observed discrepancy between wild-type BRAF and BRAF^{V600E} is caused by varied cellular stimulus, we repeated the same experiment in HEK293 cells cultured under either 4hr serum-starvation or 10% serum, representing low RAS activity and medium RAS activity, and in HCT116 colorectal cancer cell harboring oncogenic KRAS mutation, representing high RAS activity. By probing for phosphorylated MEK and ERK, we observed that, in contrast to wild-type BRAF, the replacement of Ser465/Ser467 with Ala residues didn't decrease the kinase activity of BRAF^{V600E}, suggesting that those two Ser residues are not phosphorylated in the context of BRAF^{V600E}. Although which kinase is responsible for P-loop phosphorylation needs further investigation, it is clear that BRAF^{V600E} bypasses this negative regulation mechanism in cells regardless of RAS activity.

Conclusions:

In this study, we purified FL-BRAF^{V600E} and FL-BRAF^{V600E/R509H} from mammalian cells and characterized their enzyme kinetic parameters *in vitro*. One advantage of purifying proteins from mammalian cells is that all post-translational modifications required for proper protein folding and function are maintained. We are aware of that proteins in their purified form might behave differently from native proteins in a cellular environment, thus extra caution should be taken when interpreting *in vitro* data. On the other hand, results obtained from cell-based assays typically depend on stimuli, growth cycle, cell type, and complex cellular context. A combination of cell-based assays and *in vitro* assays is necessary to reveal the complex regulation mechanism of RAF kinase. Our previous biochemical characterization of wild-type BRAF has demonstrated that intact BRAF more precisely captures the behavior of native protein and recapitulates 'paradoxical activation' *in vitro*.^[5b] Here, we extended the same strategy to study the most prevalent BRAF mutant.

Dimerization is a critical modulator of normal RAF kinase activation and involves a 'side-to-side' dimer interface within the kinase domain.^[4a] Previous cell-based studies have resulted in controversial conclusions regarding whether BRAF^{V600E} functions as a monomer or oligomer in living cells.^[26, 32] Purified FL-BRAF^{V600E} displays a higher oligomer configuration in solution, suggesting that the V600E mutation results in higher dimerization potential of BRAF. A similar mechanism has been proposed for pseudokinase mixed lineage kinase domain-like (MLKL), whose activation loop phosphorylation drives oligomerization of MLKL.^[33] Consistent with the kinetics, MD simulations of monomeric BRAF^{V600E} kinase domain demonstrate that the V600E substitution preferentially stabilizes the active conformation in which the activation loop is fully extended and the α C-helix adopts an 'IN' position. Since the 'IN' position of the α C-helix is coupled with BRAF dimerization, it explains why BRAF^{V600E} has increased oligomerization potential. Together, we provide structural and biochemical evidence to support that the 'IN' position of the α C-helix triggered by the V600E mutation actually leads to oligomerization of BRAF^{V600E}. Although an increased dimerization potential observed *in vitro* not necessarily reflects the actual oligomeric status of BRAF in cells, multiple research groups have provided solid cellular evidence supporting that BRAF is indeed oligomeric in living cells.^[16, 27, 32] In addition, BRAF^{V600E} was identified to phosphorylate MEK in a dimer-dependent manner.^[34]

Previous cell-based studies have revealed that the introduction of R509H mutation, a mutation known to severely disrupt BRAF dimers, to BRAF^{V600E} has minimal effect on kinase activity.^[26, 35] To verify whether the kinase activity of BRAF^{V600E} is dimer-independent, we compared the specific activity of purified V600E and dimer-disrupted V600E/R509H and revealed that the kinase activity of purified FL-BRAF^{V600E} is resistant to disrupted dimerization. The fact that disruption of the dimer interface with the R509H mutation didn't abolish the kinase activity of BRAF supports that BRAF^{V600E} can signal as a monomer. It seems contradictory at the first glance; however, the two conclusions are not necessarily against each other. BRAF^{V600E} can function as a monomer, but this will not rule out the possibility that BRAF^{V600E} is oligomeric in cells. We believe that insensitivity to dimer disruption is one mechanism to bypass ERK-mediated negative feedback regulation, which is known to disrupt RAF dimers under physiological conditions.

We took advantage of that FL-BRAF^{V600E/R509H} impairs dimeric formation but retains its kinase activity and investigated the role of RAF dimerization other than involvement in allosteric activation. Although the R509H mutation didn't diminish the kinase activity of V600E, it completely abolished autophosphorylation of BRAF, supporting that BRAF autophosphorylation occurs *trans*, not *cis*. Our study suggests that the activation loop occurs via *trans*-autophosphorylation; however, autophosphorylation of the activation loop does not appreciably change the catalytic activity in our experiments with the BRAF^{V600E} mutant, supporting that the V600E mutation alone is sufficient to stabilize the catalytically competent conformation, consistent with previous report that BRAF^{V600E} with Thr599A and Ser602A substitutions is as active as BRAF^{V600E}.^[5c]

Wild-type BRAF can be paradoxically activated by a number of RAF inhibitors in a RAS-dependent manner, leading to undesired MAPK-stimulated cell growth.^[10a] The underlying molecular mechanism has been the subject of extensive investigation. Previous studies have established that, as a consequence of inhibitor binding, the enhanced RAF homo- and hetero-dimerization leads to transactivation of the inhibitor-free protomer by an allosteric mechanism.^[36] Although our *in vitro* system only includes full-length BRAF and MEK substrate, purified wild-type BRAF successfully recapitulates paradoxical activation triggered by vemurafenib and dabrafenib. In contrast, purified full-length BRAF^{V600E} does not display paradoxical activation, suggesting that the kinase activity of BRAF^{V600E} is already maximal so that further activation events are unnecessary. In addition, negative allostery is believed to attribute to drug resistance. One prevalent speculation is that BRAF^{V600E} signals as a monomer *in vivo*,^[26] thus BRAF^{V600E} tumors are more sensitive to RAF inhibitors in clinics.^[9b] However, several studies support that BRAF^{V600E} is oligomeric in cells.^[32, 36-37] In light of this, we quantified the inhibition potency of dabrafenib, AZ-628, and SB-590885, three structurally diverse RAF inhibitors, against purified monomeric BRAF^{V600E/R509H} and oligomeric BRAF^{V600E}. Notably, similar inhibition profiles were obtained between BRAF^{V600E/R509H} and BRAF^{V600E}, indicating that the dimerization status of BRAF^{V600E} is not the determining factor that leads to drug sensitivity. Instead, we speculate that the V600E substitution causes distinct drug binding pattern, therefore all three categories of RAF inhibitors are compatible with dimeric BRAF^{V600E}. Apparently, the complexity of drug resistance is underestimated and further investigation is necessary to address this question.

The elevated signaling output necessary for transformation can be achieved either by enhanced enzyme activity or decreased sensitivity to negative feedback.^[38] We show here that BRAF^{V600E} is only modestly more active than wild-type BRAF in its purified form, however BRAF^{V600E} bypasses inhibitory P-loop phosphorylation in cells. We believe that the increased kinase activity of BRAF^{V600E} *in vivo*, as compared with wild-type, partially arises from the loss of the negative regulation mechanism. Previous work showed that BRAF^{V600E} and wild-type BRAF localize to macromolecular complexes with distinct composition and activity.^[32] Although it is unclear which kinase is responsible for P-loop phosphorylation, it is reasonable to presume that the macromolecular complex, in which BRAF^{V600E} resides in, protects these sites from phosphorylation.

Our findings also shed light on the molecular mechanism of allosteric activation of RAF dimers. By isolating one protomer that adopts the active conformation from a BRAF dimer, we found that the extended activation loop started forming a small helix AS-H1, which was previously identified to support the "OUT" position of the α C-helix.^[16] This conformational change seems to be particularly relevant for allosteric transactivation. Although we did not observe a significant shift of the α C-helix to firmly support that monomeric BRAF will be converted to the inactive conformation after removing the other protomer, we believe that this is due to the short simulation time (within 150 ns). Our MD simulations provide compelling structural evidence that one protomer allosterically stabilizes the active conformation of the other protomer within a dimer. This allosteric effect should be shared by the RAF kinase family. Intriguingly, several 'loss-of-

function' BRAF mutations have been identified as oncogenic drivers.^[8, 39] It has been defined that kinase-dead BRAF dimerizes with CRAF to amplify MAPK signaling and drive the proliferation of tumor cells.^[39] Since CRAF is subject to the same regulation mechanism as BRAF, it is reasonable to hypothesize that kinase-dead BRAF contributes to constitutive activation of CRAF by activating CRAF through the dimerization-mediated allosteric effect. Together, these observations identified allosteric regulation as one non-catalytic function of BRAF kinase independent of its ability to phosphorylate MEK substrates. More and more protein kinases have been revealed a broad spectrum of non-catalytic roles. How to modulate those non-catalytic functions remains challenging. Our structural simulations suggest that the activation loop and the α C-helix enable BRAF to perform the non-catalytic function, indicating that development of inhibitors that modulate these structural elements is promising in targeting the non-catalytic function of RAF kinases.

Experimental Section:

Compounds and Reagents Dabrafenib, Vemurafenib, PB-PLX7904, TAK-632, AZ-628, SB-590885 were purchased from Selleckchem. 10 mM inhibitor stocks were made in DMSO and stored at -20°C . Radioactively labeled ATP γ -P32 (#NEG002Z250UC) was purchased from Perkin Elmer. Alkaline Phosphatase, Calf Intestinal (CIP) (M0290) was purchased from NEB. Gel filtration standards (#151-1901) were purchased from Bio-Rad. Polyethylenimine Hydrochloride-MAX (PEI Max) was purchased from Polysciences (#24765). Fetal Bovine Serum (FBS) was purchased from Gemini Bio-Products (#100-602). L-glutamine (#25030-081), Dulbecco's Modified Eagle Medium (DMEM #11995-065), Trypsin-EDTA (#25300-054), OptiMEM (31985-070), PBS (10010-023) were purchased from Gibco. All other reagents were purchased without further purification.

Antibodies Anti-FLAG M2 (#F1804), anti-FLAG M2 agarose resin (#A2220), and anti-FLAG M2 magnetic resin (#M8823) were purchased from Sigma Aldrich. Talon metal affinity resin (#635501) was purchased from Takara. Profinity IMAC Ni charged resin (#156-0131) was purchased from Bio-Rad. Anti-p-MEK1/2 Ser217/221 (#9121), total-MEK 1/2 (#4694), and anti-pERK1/2 (#4370) were purchased from Cell Signaling. Actin antibody was purchased from Sigma (#A2228). Anti-p-BRAF T599 (#PA5-37497) was purchased from Invitrogen.

Plasmids *wild-type* BRAF /6x-HIS/FLAG was prepared as previously described.^[5b] BRAF-V600E/6x-HIS/FLAG and BRAF-V600E/R509H/6x-HIS/FLAG, BRAF-S465A/S467A/6x-HIS/FLAG, BRAF-V600E/S465A/S467A/6x-HIS/FLAG, BRAF-S465D/S467D/6x-HIS/FLAG, and BRAF-V600E/S465D/S467D/6x-HIS/FLAG were created using common cloning procedures with pCDNATM 4/TO (Invitrogen) as the vector.

FL-BRAF Purification All FL-BRAF constructs were expressed in HEK293F cells.^[20a] In brief, the protein cell pellet was resuspended in lysis buffer (150 mM NaCl, 20 mM HEPES pH 7.4, 1 mM Na_3VO_4 , 1 mM PMSF, 5 mM β -Glycerol Phosphate, 2.5 mM Sodium Pyrophosphate, 10 % glycerol and a CompleteTM protease inhibitor table Sigma Aldrich (# 11836153001)) on ice. The homogenous cell slurry was sonicated at 30% amplitude for 20 seconds on and 1 minute off on ice. Once lysed, the cells were centrifuged at 20,000 rpm for 40 minutes at 4°C . The supernatant was filtered with a 0.45 μm filter and applied to pre-equilibrated resin for 2-4 hrs with rotation at 4°C . The resin was washed 5 times with salt buffer alternating low (20 mM HEPES pH 7.4, 150 mM NaCl, and 10% glycerol), high (20 mM HEPES pH 7.4, 150 mM NaCl, and 10% glycerol), low, etc. To remove HSP70, an ATP wash (5 mM ATP, 20 mM MgCl_2 in low salt buffer) was used to remove HSP proteins. This ATP wash was performed 3-5 times with 10 min incubations with rotation at 4°C . After the last ATP wash, a final low salt wash was performed before elution of FL-BRAF with 1x FLAG peptide (200 $\mu\text{g}/\text{mL}$ diluted in low salt buffer) for 2-12 hours. Elutions were analyzed by SDS-Page and pooled for further purification on size exclusion chromatography on a Superdex 200 10/300 GL column (Cat # 28-9909-44). Appropriate protein fractions were concentrated with a millipore concentrator cut off 30 kDa (Cat# UFC803024) to >0.1 mg/mL and flash frozen in liquid nitrogen before storage at -80°C .

Kinase-Dead MEK1-K97M Purification Kinase-dead MEK1-K97M/6xHIS/GST protein was purified from BL21 codon plus *E. coli*. In brief, the bacterial cells were grown to an OD_{280} of 0.6-0.8 and induced with 0.5 mM IPTG at $16-18^{\circ}\text{C}$ overnight. The cells were harvested and washed with PBS then lysed in lysis buffer (Sigma Aldrich CompleteTM EDTA-Free protease inhibitor tablets (product # 11836170001), 20 mM HEPES pH 7.4, 150 mM NaCl, 10 mM β ME, 5 mM Imidazole, and 5% Glycerol) with sonication (1 mg/mL of lysozyme can be used to help with the lysis). The supernatant was added to 1 mL of equilibrated Nickel resin and incubated for 2 hours. The protein bound resin was washed with salt buffer (20 mM HEPES, 150 mM NaCl, and 5 % glycerol) as described above. MEK1 was eluted with elution buffer (200 mM imidazole, 150 mM NaCl, 20 mM HEPES pH 7.4 and 5% Glycerol) and further purified, concentrated to >0.1 mg/mL and stored as described above.

Western Blotting-Based Kinase Assay Proteins were diluted with 2x dilution buffer (25 mM HEPES pH 7.4, 0.125 mg/mL BSA and 300 mM NaCl) to a final 2x concentration of 10 nM (5 nM final) and mixed with 2x cocktail (25 mM HEPES pH 7.4, 20 mM MgCl_2 , 1 mM DTT, 50 mM β -glycerolphosphate, 200 nM MEK (100 nM final), and 2-2000 μM ATP) for 5-10 min, unless indicated that another time was used, at 30°C . The reaction was stopped with 4x loading dye and analyzed by SDS-PAGE immunoblotting. The PVDF membranes were probed with the appropriate primary and HRP-tagged secondary antibodies followed by a chemiluminescent incubation. Quantitative analyses of the immunoblots were executed with ImageJ software.

Radioactive Spin-Column Assay RAF was diluted in 2x dilution buffer to 0-400 nM (0-200 nM final) and mixed with 2x cocktail (25 mM HEPES pH 7.4, 20 mM MgCl_2 , 1 mM DTT, 50 mM β -glycerolphosphate, 10% glycerol, 700 nM MEK (350 nM), 1-200 μM non-radioactive ATP and 1 $\mu\text{Ci}/\text{reaction}$ buffer radioactive ATP γ -P32) for 5-20 min at 30°C . The reaction was quenched with 100 mM EDTA. The samples were loaded onto a 30 kDa spin column Omega (part # OD030C35) and washed with phosphate buffer (25 mM Mono-/475 mM di-basic phosphate, and 250 mM NaCl). These columns were added to scintillation fluid (reference contained just scintillation fluid and the reaction buffer). The total radioactivity in the reference and sample vials were measured with a scintillation counter and calculated for V/E.

BRAF ELISA Inhibition Assays Pierce glutathione coated plates (cat. # 15240) were washed with 1x THBS (25 mM HEPES pH 7.4, 140 mM NaCl, 0.05% Tween-20) then incubated with GST-MEK (0.0025 mg/mL final) for >2 hrs with shaking. Concurrently, 100x inhibitor was added to 2x RAF (5 nM final) with shaking for 1 hr. Proceeding this incubation, 2x cocktail buffer, containing ATP, was added to the glutathione-coated plate followed by the addition of 2x RAF/inhibitor and incubated at 30°C for 15 min. All wells were washed with 1x THBS and incubated for 5 minutes at RT (2x), then primary anti-pMEK (1:5,000) was added to the plate for one hour. The plate was then washed with 1x THBS twice and secondary anti-rabbit HRP (1:5,000) was added to the plate for one hour. The

plate was washed three times with wash buffer. On the final wash, Pierce super signal pico chemiluminescent substrate reagents were mixed together (cat. # 37070). The luminescence was measured on Biotek Synergy 2.

Transient Transfection into Mammalian Cells HEK293 cells were a gift from Dr. Catherine Moore and HCT116 cancer cells were a gift from Dr. Jean-Francois Jasmine. Transfections were performed by plating 1 million cells in DMEM supplemented with 10% FBS and 1% L-glutamine on a 6-well plate. These cells were incubated at 37°C with 5% CO₂ for 24 hours or until the cells reach a confluency of 40-60%. DNA (1-3 µg) was mixed with PEI-MAX in a 1:3 ratio in opti-MEM at RT for ~25 minutes. Before plating, old DMEM was aspirated out and 1.8 mL of fresh DMEM was added to the plate followed by 200 µL of the DNA/PEI-MAX solution. After 24-48 hrs, the cells were washed with cold PBS then harvested and lysed with 4% SDS. Homogenizer columns were used to separate the supernatant from the pellet.

Calf-Intestinal Phosphatase Dephosphorylation Assay CIP contained the storage buffer with Mg²⁺ and Zn²⁺ was diluted in 2x dilution buffer. 4x BRAF (5 nM final) was incubated with 4x CIP for 20 minutes at RT, then 4x β-GP (200 mM) was added and incubated for 20 minutes at 4°C. After this incubation, 4x BRAF/CIP/β-GP were added to 4x cocktail and incubated 5-10 minutes at 30°C. For the control, BRAF/CIP/β-GP were all mixed together in the first step and incubated at RT for 20 minutes, then on ice for 20 minutes, and followed by 4x cocktail buffer. The reactions were loaded on a 10% SDS-Page gel and subjected to immunoblotting.

Molecular Dynamics Simulations. Each crystal structure selected for simulation was cleaned up and solvated in a periodic box of explicit TIP3P water molecules. The ff14SB force field^[40] was applied to the protein. All MD simulations were carried out using GPU-implemented AMBER16.^[41] All systems were equilibrated using the same procedure involving solvent minimization, heating and NPT simulation at 1 atm and 300K. Production runs using the NVT ensemble at 300K were then carried out for 100 to 200 ns per system. The trajectories were then analyzed using the cptraj program in the AMBER16 package in terms of hydrogen bond interactions, RMSD, distance etc. as discussed.

In-Gel Radioactive Assay A 2x cocktail buffer (25 mM HEPES pH 7.4, 20 mM MgCl₂, 50 mM β- glycerolphosphate, 1mM DTT, 4 mM Na₃VO₄, 200 uM ATP, and 1 uCi radioactive ATP) was mixed with 2x BRAF (200 nM final). 700 nM MEK was spiked into the cocktail buffer for experiments that contained MEK/ATP. This was incubated for 30 minutes at RT before being transferred to SDS-Page, dried, and imaged on a STORM imager.

Accession Codes.

BRAF: Uniprot ID# P15056

MEK1: Uniprot ID# Q02750

Acknowledgements:

The study was funded by the W.W. Smith Charitable Fund to Z. Wang and the Spiers Fellowship to N. Cope.

Keywords: BRAF, trans autophosphorylation, dimerization, drug resistance, molecular dynamics**References**

- [1] J. Downward, *Nature reviews. Cancer* **2003**, *3*, 11-22.
- [2] H. Lavoie, M. Therrien, *Nature Reviews Molecular Cell Biology* **2015**, *16*, 281.
- [3] M. Holderfield, M. M. Deuker, F. McCormick, M. McMahon, *Nature reviews. Cancer* **2014**, *14*, 455-467.
- [4] aT. Rajakulendran, M. Sahmi, M. Lefrancois, F. Sicheri, M. Therrien, *Nature* **2009**, *461*, 542-545; bC. K. Weber, J. R. Slupsky, H. A. Kalmes, U. R. Rapp, *Cancer Res* **2001**, *61*, 3595-3598; cJ. Hu, Edward C. Stites, H. Yu, Elizabeth A. Germino, Hiruy S. Meharena, Philip J. S. Stork, Alexandr P. Kornev, Susan S. Taylor, Andrey S. Shaw, *Cell* **2013**, *154*, 1036-1046.
- [5] aB. H. Zhang, K. L. Guan, *Embo j* **2000**, *19*, 5429-5439; bN. Cope, C. Candelora, K. Wong, S. Kumar, H. Nan, M. Grasso, B. Novak, Y. Li, R. Marmorstein, Z. Wang, *Chembiochem : a European journal of chemical biology* **2018**; cM. Köhler, M. Röring, B. Schorch, K. Heilmann, N. Stickel, G. J. Fiala, L. C. Schmitt, S. Braun, S. Ehrenfeld, F. M. Uhl, T. Kaltenbacher, F. Weinberg, S. Herzog, R. Zeiser, W. W. Schamel, H. Jumaa, T. Brummer, *The EMBO Journal* **2016**, *35*, 143-161.
- [6] aM. J. Garnett, S. Rana, H. Paterson, D. Barford, R. Marais, *Molecular Cell* **2005**, *20*, 963-969; bC. S. Mason, C. J. Springer, R. G. Cooper, G. Superti-Furga, C. J. Marshall, R. Marais, *EMBO J* **1999**, *18*, 2137-2148.
- [7] H. Davies, G. R. Bignell, C. Cox, P. Stephens, S. Edkins, S. Clegg, J. Teague, H. Woffendin, M. J. Garnett, W. Bottomley, N. Davis, E. Dicks, R. Ewing, Y. Floyd, K. Gray, S. Hall, R. Hawes, J. Hughes, V. Kosmidou, A. Menzies, C. Mould, A. Parker, C. Stevens, S. Watt, S. Hooper, R. Wilson, H. Jayatilake, B. A. Gusterson, C. Cooper, J. Shipley, D. Hargrave, K. Pritchard-Jones, N. Maitland, G. Chenevix-Trench, G. J. Riggins, D. D. Bigner, G. Palmieri, A. Cossu, A. Flanagan, A. Nicholson, J. W. C. Ho, S. Y. Leung, S. T. Yuen, B. L. Weber, H. F. Seigler, T. L. Darrow, H. Paterson, R. Marais, C. J. Marshall, R. Wooster, M. R. Stratton, P. A. Futreal, *Nature* **2002**, *417*, 949-954.
- [8] P. T. C. Wan, M. J. Garnett, S. M. Roe, S. Lee, D. Niculescu-Duvaz, V. M. Good, C. G. Project, C. M. Jones, C. J. Marshall, C. J. Springer, D. Barford, R. Marais, *Cell* **2004**, *116*, 855-867.
- [9] aK. T. Flaherty, J. R. Infante, A. Daud, R. Gonzalez, R. F. Kefford, J. Sosman, O. Hamid, L. Schuchter, J. Cebon, N. Ibrahim, R. Kudchadkar, H. A. Burris, G. Falchook, A. Algazi, K. Lewis, G. V. Long, I. Puzanov, P. Lebowitz, A. Singh, S. Little, P. Sun, A. Allred, D. Ouellet, K. B. Kim, K. Patel, J. Weber, *New England Journal of Medicine* **2012**, *367*, 1694-1703; bG. Bollag, P. Hirth, J. Tsai, J. Zhang, P. N. Ibrahim, H. Cho, W. Spevak, C. Zhang, Y. Zhang, G. Habets, E. A. Burton, B. Wong, G. Tsang, B. L. West, B. Powell, R. Shellooe, A. Marimuthu, H. Nguyen, K. Y. Zhang, D. R. Artis, J. Schlessinger, F. Su, B. Higgins, R. Iyer, K. D'Andrea, A. Koehler, M. Stumm, P. S. Lin, R. J. Lee, J. Grippo, I. Puzanov, K. B. Kim, A. Ribas, G. A. McArthur, J. A. Sosman, P. B. Chapman, K. T. Flaherty, X. Xu, K. L. Nathanson, K. Nolop, *Nature* **2010**, *467*, 596-599.
- [10] aP. I. Poulikakos, C. Zhang, G. Bollag, K. M. Shokat, N. Rosen, *Nature* **2010**, *464*, 427-430; bG. Hatzivassiliou, K. Song, I. Yen, B. J. Brandhuber, D. J. Anderson, R. Alvarado, M. J. C. Ludlam, D. Stokoe, S. L. Gloor, G. Vigers, T. Morales, I. Aliagas, B. Liu, S. Sideris, K. P. Hoeflich, B. S. Jaiswal, S. Seshagiri, H. Koeppen, M. Belvin, L. S. Friedman, S. Malek, *Nature* **2010**, *464*, 431-435.
- [11] B. Agianian, E. Gavathiotis, *J Med Chem* **2018**, *61*, 5775-5793.

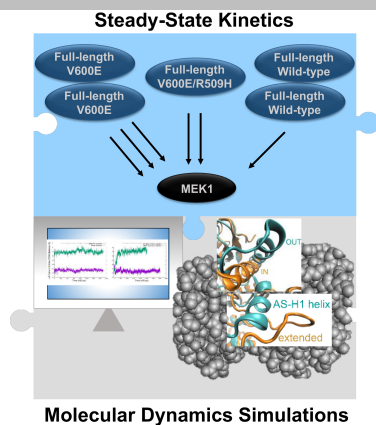
- [12] S. S. Taylor, A. P. Kornev, *Trends in biochemical sciences* **2011**, *36*, 65-77.
- [13] J. E. Kung, N. Jura, *Structure* **2016**, *24*, 7-24.
- [14] Z. Karoulia, Y. Wu, Tamer A. Ahmed, Q. Xin, J. Bollard, C. Krepler, X. Wu, C. Zhang, G. Bollag, M. Herlyn, James A. Fagin, A. Lujambio, E. Gavathiotis, Poulidakos I. Poulidakos, *Cancer Cell* **2016**, *30*, 485-498.
- [15] Z. Karoulia, E. Gavathiotis, P. I. Poulidakos, *Nature reviews. Cancer* **2017**, *17*, 676-691.
- [16] N. Thevakumaran, H. Lavoie, D. A. Critton, A. Tebben, A. Marinier, F. Sicheri, M. Therrien, *Nat Struct Mol Biol* **2015**, *22*, 37-43.
- [17] Jacob R. Haling, J. Sudhamsu, I. Yen, S. Sideris, W. Sandoval, W. Phung, Brandon J. Bravo, Anthony M. Giannetti, A. Peck, A. Masselot, T. Morales, D. Smith, Barbara J. Brandhuber, Sarah G. Hymowitz, S. Malek, *Cancer Cell* **2014**, *26*, 402-413.
- [18] M. Holderfield, H. Merritt, J. Chan, M. Wallroth, L. Tandeske, H. Zhai, J. Tellew, S. Hardy, M. Hekmat-Nejad, Darrin D. Stuart, F. McCormick, Tobi E. Nagel, *Cancer Cell* **2013**, *23*, 594-602.
- [19] R. Barouch-Bentov, J. Che, C. C. Lee, Y. Yang, A. Herman, Y. Jia, A. Velentza, J. Watson, L. Sternberg, S. Kim, N. Ziaee, A. Miller, C. Jackson, M. Fujimoto, M. Young, S. Batalov, Y. Liu, M. Warmuth, T. Wiltshire, M. P. Cooke, K. Sauer, *Mol Cell* **2009**, *33*, 43-52.
- [20] aC. Qiu, M. K. Tarrant, T. Boronina, P. A. Longo, J. M. Kavran, R. N. Cole, P. A. Cole, D. J. Leahy, *Biochemistry* **2009**, *48*, 6624-6632; bZ. Wang, C. Candelora, *Methods in molecular biology (Clifton, N.J.)* **2017**, *1487*, 23-33.
- [21] E. W. Joseph, C. A. Pratilas, P. I. Poulidakos, M. Tadi, W. Wang, B. S. Taylor, E. Halilovic, Y. Persaud, F. Xing, A. Viale, J. Tsai, P. B. Chapman, G. Bollag, D. B. Solit, N. Rosen, *Proceedings of the National Academy of Sciences* **2010**, *107*, 14903.
- [22] M. Grasso, M. A. Estrada, K. N. Berrios, J. D. Winkler, R. Marmorstein, *J Med Chem* **2018**, *61*, 5034-5046.
- [23] F. A. Karreth, G. M. DeNicola, S. P. Winter, D. A. Tuveson, *Molecular Cell* **2009**, *36*, 477-486.
- [24] H. Lavoie, J. J. Li, N. Thevakumaran, M. Therrien, F. Sicheri, *Trends Biochem Sci* **2014**, *39*, 475-486.
- [25] J. Qin, P. Xie, C. Ventocilla, G. Zhou, A. Vultur, Q. Chen, Q. Liu, M. Herlyn, J. Winkler, R. Marmorstein, *J Med Chem* **2012**, *55*, 5220-5230.
- [26] P. I. Poulidakos, Y. Persaud, M. Janakiraman, X. Kong, C. Ng, G. Moriceau, H. Shi, M. Atefi, B. Titz, M. T. Gabay, M. Salton, K. B. Dahlman, M. Tadi, J. A. Wargo, K. T. Flaherty, M. C. Kelley, T. Misteli, P. B. Chapman, J. A. Sosman, T. G. Graeber, A. Ribas, R. S. Lo, N. Rosen, D. B. Solit, *Nature* **2011**, *480*, 387-390.
- [27] M. Röring, R. Herr, G. J. Fiala, K. Heilmann, S. Braun, A. E. Eisenhardt, S. Halbach, D. Capper, A. von Deimling, W. W. Schamel, D. N. Saunders, T. Brummer, *The EMBO Journal* **2012**, *31*, 2629-2647.
- [28] M. Grasso, M. A. Estrada, C. Ventocilla, M. Samanta, J. Maksimoska, J. Villanueva, J. D. Winkler, R. Marmorstein, *ACS Chem Biol* **2016**, *11*, 2876-2888.
- [29] M. J. Vido, K. Le, E. J. Hartsough, A. E. Aplin, *Cell Rep* **2018**, *25*, 1501-1510 e1503.
- [30] S. B. Peng, J. R. Henry, M. D. Kaufman, W. P. Lu, B. D. Smith, S. Vogeti, T. J. Rutkoski, S. Wise, L. Chun, Y. Zhang, R. D. Van Horn, T. Yin, X. Zhang, V. Yadav, S. H. Chen, X. Gong, X. Ma, Y. Webster, S. Buchanan, I. Mochalkin, L. Huber, L. Kays, G. P. Donoho, J. Walgren, D. McCann, P. Patel, I. Conti, G. D. Plowman, J. J. Starling, D. L. Flynn, *Cancer Cell* **2015**, *28*, 384-398.
- [31] C. Zhang, W. Spevak, Y. Zhang, E. A. Burton, Y. Ma, G. Habets, J. Zhang, J. Lin, T. Ewing, B. Matusow, G. Tsang, A. Marimuthu, H. Cho, G. Wu, W. Wang, D. Fong, H. Nguyen, S. Shi, P. Womack, M. Nespi, R. Shellooe, H. Carias, B. Powell, E. Light, L. Sanftner, J. Walters, J. Tsai, B. L. West, G. Visor, H. Rezaei, P. S. Lin, K. Nolop, P. N. Ibrahim, P. Hirth, G. Bollag, *Nature* **2015**, *526*, 583-586.
- [32] B. Diedrich, K. T. Rigbolt, M. Röring, R. Herr, S. Kaeser-Pebernard, C. Gretzmeier, R. F. Murphy, T. Brummer, J. Dengjel, *The EMBO journal* **2017**, *36*, 646-663.

- [33] H. Wang, L. Sun, L. Su, J. Rizo, L. Liu, L. F. Wang, F. S. Wang, X. Wang, *Mol Cell* **2014**, *54*, 133-146.
- [34] J. Yuan, W. H. Ng, P. Y. P. Lam, Y. Wang, H. Xia, J. Yap, S. P. Guan, A. S. G. Lee, M. Wang, M. Baccharini, J. Hu, *Oncogene* **2018**, *37*, 5719-5734.
- [35] Z. Yao, N. M. Torres, A. Tao, Y. Gao, L. Luo, Q. Li, E. de Stanchina, O. Abdel-Wahab, D. B. Solit, P. I. Poulikakos, N. Rosen, *Cancer Cell* **2015**, *28*, 370-383.
- [36] H. Lavoie, N. Thevakumaran, G. Gavory, J. J. Li, A. Padeganeh, S. Guiral, J. Duchaine, D. Y. L. Mao, M. Bouvier, F. Sicheri, M. Therrien, *Nat Chem Biol* **2013**, *9*, 428-436.
- [37] A. K. Freeman, D. A. Ritt, D. K. Morrison, *Small GTPases* **2013**, *4*, 180-185.
- [38] M. A. Lemmon, D. M. Freed, J. Schlessinger, A. Kiyatkin, *Cell* **2016**, *164*, 1172-1184.
- [39] P. Nieto, C. Ambrogio, L. Esteban-Burgos, G. Gomez-Lopez, M. T. Blasco, Z. Yao, R. Marais, N. Rosen, R. Chiarle, D. G. Pisano, M. Barbacid, D. Santamaria, *Nature* **2017**, *548*, 239-243.
- [40] J. A. Maier, C. Martinez, K. Kasavajhala, L. Wickstrom, K. E. Hauser, C. Simmerling, *Journal of chemical theory and computation* **2015**, *11*, 3696-3713.
- [41] R. M. B. D.A. Case, D.S. Cerutti, T.E. Cheatham, III, T.A. Darden, R.E. Duke, T.J. Giese, H. Gohlke, A.W. Goetz, N. Homeyer, S. Izadi, P. Janowski, J. Kaus, A. Kovalenko, T.S. Lee, S. LeGrand, P. Li, C. Lin, T. Luchko, R. Luo, B. Madej, D. Mermelstein, K.M. Merz, G. Monard, H. Nguyen, H.T. Nguyen, I. Omelyan, A. Onufriev, D.R. Roe, A. Roitberg, C. Sagui, C.L. Simmerling, W.M. Botello-Smith, J. Swails, R.C. Walker, J. Wang, R.M. Wolf, X. Wu, L. Xiao and P.A. Kollman, **2016**.

FULL PAPER

Oncogenic BRAF:

BRAF^{V600E} was subjected to steady-state kinetics and MD simulations analyses to shed light on the features that ascribe to its tumorigenesis. Full-length BRAF^{V600E}, BRAF^{V600E/R509H}, BRAF^{WT} activities were compared. The kinase domain was used in molecular dynamics simulations to explain the dimer independent activity of BRAF^{V600E} and the increased dimerization of purified BRAF^{V600E}.



Nicholas Cope, Borna Novak, Christine Candelora, Kenneth Wong, Maria Cavallo, Amber Gunderwala, Zhiwei Liu, Yana Li, and Zhihong Wang

Biochemical Characterization of Full-length Oncogenic BRAF^{V600E} Together with Molecular Dynamics Simulations Provide Insight into the Activation and Inhibition Mechanisms of RAF Kinases

Keyword: BRAF, trans autophosphorylation, dimerization, drug resistance, molecular dynamics